CrossMark

MRS Advances © 2018 Materials Research Society
DOI: 10.1557/adv.2018.418

Downloaded from https://www.cambridge.org/core. University of Warwick, on 21 May 2018 at 01:52:47, subject to the Cambridge Core terms of use, available at https://www.cambridge.org/core/terms. https://doi.org/10.1557/adv.2018.418

Efficient Approaches on Photochemical CO_2 Reduction to Alcohol by Solar Light with Functional Multi-layered Membrane Catalysts

Myung Jong Kang and Young Soo Kang*

Korea Center for Artificial Photosynthesis, Department of Chemistry, Sogang University, Seoul, 04107, Republic of Korea

ABSTRACT

Simple and efficient approach for artificial photosynthesis of CO_2 reduction into ethanol with flexible functional multi-layered membrane catalysts is suggested. The g-C_3N_4 and $BiVO_4$ particle were synthesized by self-condensation and hydrothermal method. g-C_3N_4 membrane catalyst and g-C_3N_4/$BiVO_4$ layered membrane catalyst were fabricated by casting and shaping of Nafion polymer mixture. XRD, FT-IR and XPS analyses proved that the intrinsic properties of g-C_3N_4 and $BiVO_4$ were maintained after fabricating flexible functional multi-layered membrane catalyst. The interfacial contact between g-C_3N_4 and $BiVO_4$ particles in flexible membrane catalyst for efficient transport of photogenerated electron was revealed by TEM and photoelectrochemical analysis. Finally, photochemical CO_2 reduction reaction was performed with flexible functional multi-layered membrane catalysts. The g-C_3N_4 membrane catalysts produced 147 μM of ethanol during 12 hrs of CO_2 reduction reaction while the g-C_3N_4/$BiVO_4$ layered membrane catalysts produced 256 μM of ethanol during 12 hrs of CO_2 reduction reaction. This is due to the higher solar light harvesting and efficient hole-charge separation from functional multi-layered $BiVO_4$ membrane catalyst leading to the higher electron transport rate to g-C_3N_4 membrane catalysts, promoting the CO_2 reduction reaction on the surface of g-C_3N_4 membrane catalyst.

INTRODUCTION

Efficient utilization of solar energy is one of the most critical issues in environmental friendly renewable energy. The solar energy can be converted into heat energy, electrical energy and chemical energy by solar heat plates, solar cells and photosynthesis, respectively. The solar cell can utilize solar radiation more efficiently and can adjust power easily by changing connection system of modules. Because of difficulty to store the electricity produced by solar cell, direct synthesis of fuels utilizing the solar light become a new generation technology to convert solar energy. The first approach was started with the discovery of photocatalytic effects of TiO_2 by Fujishima.[1] With the photocatalytic effects of semiconductors, hydrogen and oxygen can be produced through solar water splitting.[2-4] The semiconductors with photocatalytic activities such as TiO_2,[5-7] ZnO,[8-10] $BiVO_4$,[11, 12] GaAs,[13, 14]

WO_3 [15-17] and CdS[18, 19] etc. were used for solar water splitting system and the highest solar to hydrogen efficiency (STF) was recorded as 8.2% with multi-array of c-Si, Fe_2O_3 and $BiVO_4$ with co-catalysts system.[20] The hydrogen, produced through the solar water splitting reaction, is renewable energy because it produces water as a combustion product. However, inappropriate physical properties of hydrogen for storing and transporting such as low boiling point (~ 20 K) and low density (0.089 g/L) make hydrogen difficult to be used as a fuel. To overcome these drawbacks of hydrogen as a fuel and reduce the amount of CO_2 in atmosphere as the solutions for the greenhouse effect, researches on converting CO_2 to liquid fuels like methanol, ethanol, formaldehyde and formic acid by solar energy through the photocatalytic systems, which is called as the artificial photosynthesis, are going under active. However, most of CO_2 reduction products of artificial photosynthesis process are CO and methane, with low solar to fuel efficiency less than 1%.[21] Recently, photoelectrochemical CO_2 reduction by photocatalytic electrode and photochemical CO_2 reduction by photocatalytic powder based artificial photosynthesis system have been studied widely.[22],[23-25] Among various kinds of approaches, the approaches with Z-scheme, which uses two photocatalysts to mimic natural photosynthesis, is considered as a promising strategies on photochemical artificial photosynthesis system.[26, 27] However, the major problems of photochemical artificial photosynthesis system are that it is hard to prevent re-oxidation of CO_2 reduction products. For instance, methanol is good hole scavenger material, so it undergoes re-oxidation process by reacting with holes which were generated by light induced electron-hole charge separation in powder based photocatalysts. Because of re-oxidation process of CO_2 reduction products, solar to fuel efficiency in most of powder based photochemical system limited on ~1%. In case of photoelectrochemical system, the re-oxidation of CO_2 reduction products is prohibited by separating water splitting half reaction and CO_2 reduction half reaction within membrane like Nafion. However, due to the complicate system which is consisted of anode, cathode and separating membrane, it increases total size and volume of photoelectrochemical artificial photosynthesis system. The increased volume of photoelectrochemical artificial photosynthesis system causes low proton mobility through the electrolyte solution, resulted in a low CO_2 reduction reaction rate with low solar to fuel efficiency.

In this report, we suggest the facile and simple artificial photosynthesis system which can prohibit the re-oxidation of CO_2 reduction products with compact size system for better proton mobility by layer structured membrane catalysts. Within layered structure of oxygen evolution membrane and CO_2 reduction membrane, we successfully reduced CO_2 to the ethanol as the dominant artificial photosynthesis products, prohibiting re-oxidation of CO_2 reduction products and increased proton mobility through the membrane.

EXPERIMENTAL DETAILS

Synthetic methods

Dicyandiamide (Sigma-Aldrich) was self-condensed in furnace with air flow condition at 823 K for 4 hrs with 2 K/min ramping rate to make bulk state g-C_3N_4. The bulk state g-C_3N_4 was grinded before used. $BiVO_4$ particle was synthesized by 1.4 g of NH_4VO_3 (Sigma-Aldrich), 5.8 g of $Bi(NO_3)_3$•$5H_2O$ (Sigma-Aldrich) and 3 g of urea (Sigma-Aldrich) were dissolved in 50 mL of 2.0 M nitric acid solution. After 30 min stirring, the solution was transferred into Teflon-lined autoclave and reacted at 453 K for 24 hrs. The product was collected and washed by centrifuge, dried at 353 K oven. The bulk state $BiVO_4$ was grinded by mortar before used.

Downloaded from https://www.cambridge.org/core. University of Warwick, on 21 May 2018 at 01:52:47, subject to the Cambridge Core terms of use, available at https://www.cambridge.org/core/terms. https://doi.org/10.1557/adv.2018.418

Fabrication of C_3N_4, $bivo_4$ membrane and $bivo_4/C_3N_4$ multi-layered membrane

A 1 ml of Nafion solution (20 wt%, IKO Chemical) was mixed with 0.2 g of g-C_3N_4 powder for g-C_3N_4-Nafion mixed solution. A 1 ml of Nafion solution was mixed with 0.4 g of $BiVO_4$ powder for $BiVO_4$-Nafion mixed solution. For fabricating g-C_3N_4 membrane and $BiVO_4$ membrane, solutions were well grinded by mortar and mixtures were casted and shaped at room temperature by pressing. The g-C_3N_4/$BiVO_4$ multi-layered membrane was fabricated by pressing with high-temperature applied. Both g-C_3N_4 membrane and $BiVO_4$ membrane were stacked up and pressed with 40 psi for 5 min at 383 K.

Artificial Photosynthesis Reaction with Multi-layered Membrane Catalysts

The photochemical artificial photosynthesis reaction was performed with home-made photochemical reactor. The CO_2 gas was used to purge into the reaction cell with a flow rate of 20 sccm. A 0.5 M $KHCO_3$ solution was used as an electrolyte. The one-sun illumination (AM1.5 G, 100 mW/cm^2) was applied to the membrane for efficient electron-hole separation with a 300-W Xe lamp (HAL-320, Ashai Spectra, Japan).

Characterization

The surface morphology and cross-sectional images of the g-C_3N_4, $BiVO_4$, g-C_3N_4/ $BiVO_4$ multi-layered membrane catalyst were investigated by SEM (Hitachi Horiba S-4300) operated with a 20-kV incident electron beam with EDS analysis. The electrochemical properties of membrane catalyst measured by potentiostat (VSP-3, Biologics Ltd.) with 2 electrode system and 0.5 M potassium bicarbonate solution. To prevent short-circuit current, the connection points of membrane with Cu external wire and electrolyte were sealed by epoxy resin. The crystal structure was defined with XRD (Rigaku Ultima 2000) with scan speed of 0.5 °/min in the range of 20° ~ 80° in 2θ mode using Cu Kα radiation. Infrared spectroscopy was measured by Thermo Nicolet iS5. Binding state of g-C_3N_4, $BiVO_4$, g-C_3N_4/ $BiVO_4$ layered membrane was investigated by X-ray photoelectron spectroscopy (XPS, Kratos Ultra DLD) with Al Kα radiation. After the photochemical CO_2 reduction reactions, the liquid products in the cathode cell were collected and analysed by NMR (Varian 400 MHz) with water suppression. The CO_2 reduction products was qualified and quantified by standard calibration curves with chemical shift position and area of standard materials' NMR peak.

Downloaded from https://www.cambridge.org/core. University of Warwick, on 21 May 2018 at 01:52:47, subject to the Cambridge Core terms of use, available at https://www.cambridge.org/core/terms.
https://doi.org/10.1557/adv.2018.418

RESULTS AND DISCUSSION

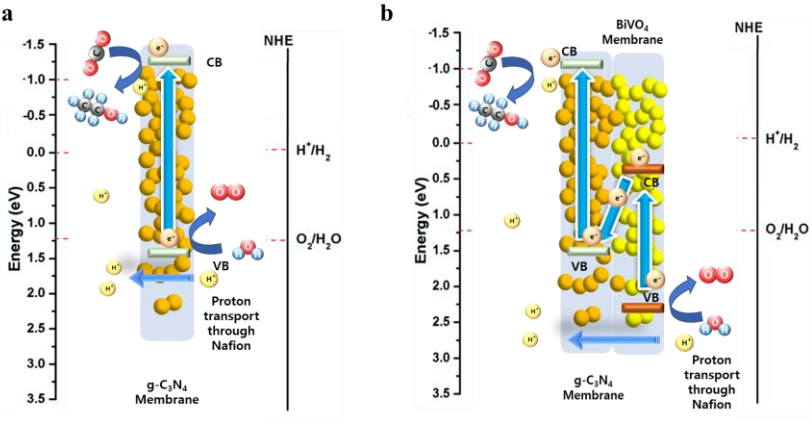

Figure 1. Schematic drawings on the (a) g-C_3N_4 membrane and (b) g-C_3N_4/$BiVO_4$ multi-layered membrane

The schematic drawings of artificial photosynthesis of CO_2 reduction reaction by the membrane catalysts is shown in Figure 1. The major concept of artificial photosynthesis of CO_2 reduction reaction through the g-C_3N_4/$BiVO_4$ multi-layered membrane is that the multi-layered membrane catalyst offers the water oxidation reaction site, CO_2 reduction reaction site, electron-proton transport from water oxidation site to CO_2 reduction site simultaneously and the artificial photosynthesis reaction occurs by incident sunlight to the membrane catalysts. Although the band position of g-C_3N_4 membrane catalyst is able to perform both water splitting reaction and CO_2 reduction reaction (Figure 1a), the catalytic water splitting efficiency of g-C_3N_4 is low.[28] By constructing multi-layered membrane catalyst with g-C_3N_4 and $BiVO_4$, g-C_3N_4 gives complementary effect on the low water splitting efficiency within a Z-scheme electron transport pathway by getting more electron excitation from the valence energy level of g-C_3N_4 and the suppression of charge recombination (Figure 1b).

Downloaded from https://www.cambridge.org/core. University of Warwick, on 21 May 2018 at 01:52:47, subject to the Cambridge Core terms of use, available at https://www.cambridge.org/core/terms. https://doi.org/10.1557/adv.2018.418

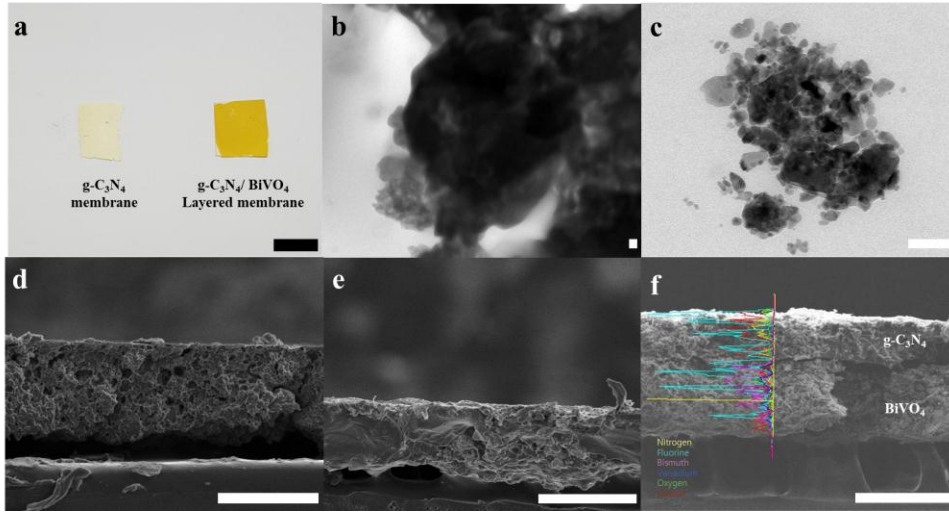

Figure 2. (a) Optical images of g-C_3N_4 membrane and g-C_3N_4/$BiVO_4$ multi-layered membrane (the scale bar is 1 cm). TEM images of (b) g-C_3N_4 membrane and (c) $BiVO_4$ membrane (all scale bar is 100 nm). Cross-sectional SEM images of (d) $BiVO_4$ membrane, (e) g-C_3N_4 membrane and (f) g-C_3N_4/$BiVO_4$ multi-layered membrane and line-profile EDS analysis. (all scale bar is 100 μm).

Both g-C_3N_4 membrane catalyst and g-C_3N_4/$BiVO_4$ multi layered membrane catalyst were fabricated in 1 cm x 1 cm scale. The optical images of g-C_3N_4 membrane catalyst and g-C_3N_4/$BiVO_4$ multi layered membrane catalyst are shown in Figure 2a. For the efficient electron transfer from water oxidation site to CO_2 reduction site, both g-C_3N_4 and $BiVO_4$ particles should be well attached to each other to maintain the membrane structure. This is important due to intrinsic properties of Nafion polymer which is excellent media for the proton transport via diffusion through sulfonate ions inside the polymer backbones.[29] In TEM images of g-C_3N_4 membrane (Figure 2b) and $BiVO_4$ membrane (Figure 2c), each particle of g-C_3N_4 and $BiVO_4$ was well contacted with each other to make an efficient electron transport pathway through the membrane and Nafion polymer was filled between the particles to make an efficient proton transport pathway through the membrane. The thickness of g-C_3N_4 and $BiVO_4$ membrane catalysts were determined as ~ 80 μm and ~ 100 μm, respectively, with cross sectional SEM images (Figure 2d and e). The line profiled EDS analysis was confirmed that the total thickness of g-C_3N_4/$BiVO_4$ multi-layered membrane catalysts was ~ 180 μm, while the thickness of g-C_3N_4 membrane catalysts was ~80 μm and the thickness of $BiVO_4$ membrane catalysts was ~ 100 μm (Figure 2f).

To confirm whether each photocatalyst in the membrane keeps its own property during fabricating the membrane catalysts or not, XRD was measured for the configuration of crystal structure of photocatalysts and FT-IR spectra were obtained for the function groups of g-C_3N_4 and $BiVO_4$. In the XRD pattern of pure Nafion membrane in Figure 3a, the peak at $2\theta = 18$ ° and broad peak at around 40 ° were well matched with the previous report on the XRD pattern of Nafion 117 membrane.[30] In case of XRD pattern of g-C_3N_4 in Figure 3b, most of peaks except the pristine Nafion 117 membrane were well matched with the previous XRD pattern of g-C_3N_4 (JCPDS #50-1250).

Downloaded from https://www.cambridge.org/core. University of Warwick, on 21 May 2018 at 01:52:47, subject to the Cambridge Core terms of use, available at https://www.cambridge.org/core/terms. https://doi.org/10.1557/adv.2018.418

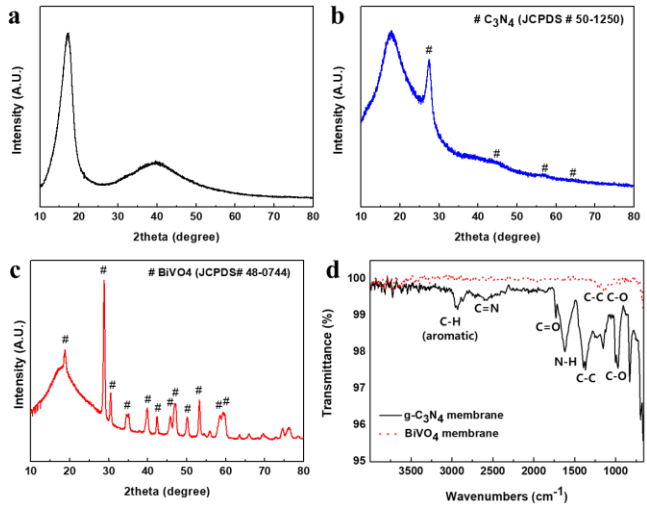

Figure 3. XRD patterns of (a) Nafion membrane, (b) g-C_3N_4 membrane and (c) $BiVO_4$ membrane catalysts. (d) IR spectra of g-C_3N_4/$BiVO_4$ multi-layered membrane with different IR incident direction.

However, in XRD pattern of $BiVO_4$, the XRD peak of pristine Nafion 117 membrane was broadened while the other peaks were well matched with the previous XRD pattern of $BiVO_4$ (JCPDS #48-0744). This is due to the higher crystallinity $BiVO_4$ particle than Nafion 117 membrane, resulting in peak broadening of Nafion 117 at around 18°. By measuring FT-IR spectra of g-C_3N_4 (Figure 3d), it was confirmed that the g-C_3N_4 membrane catalyst still keeps the original structure of g-C_3N_4 with C=N stretching from the nitrogen of g-C_3N_4 (2600 cm^{-1}), aromatic C-H stretching from nitrogen contained hexagonal ring structure of g-C_3N_4 (3100 cm^{-1}) and other C-N stretching, C=O stretching by comparing with the previous FT-IR spectrum of g-C_3N_4.[31] However, in the FT-IR spectrum of $BiVO_4$ membrane, only C-C stretching, C-O stretching and C-F stretching peaks were originated from Nafion polymer backbones.

In the artificial photosynthesis reaction, solar water splitting reaction and CO_2 reduction reaction for solar fuel generation (*i.e.* methanol) occur simultaneously as two main half-reactions. The reaction equation of each half reaction is like below:

$$H_2O + h^+_{cat.} \rightarrow O_2 + H^+ \ (solar\ water\ splitting)$$

$$CO_2 + 6\, e^-_{cat.} + 6\, H^+_{trans.} \underset{cat.}{\longrightarrow} CH_3OH + H_2O \ (CO_2\ reduction\ for\ solar\ fuel\ production)$$

Where the $h^+_{cat.}$ is generated hole by electron-hole charge separation of photocatalyst, $e^-_{cat.}$ is generated electron by electron-hole charge separation of photocatalyst and $H^+_{trans.}$ stands for the proton generated by solar water splitting reaction and were transported to CO_2 reduction reaction site through Nafion polymer membrane. It is well known that Bi atom takes an important role in water splitting reaction when $BiVO_4$ involved as the photocatalyst by offering proper angles of O-Bi-V structure for water molecule adsorption and changing coordination state from Bi^{4+} to Bi^{3+} by accepting electrons from water.[11] In CO_2 reduction reaction, it was already reported that N-heterocyclic 2-D

Downloaded from https://www.cambridge.org/core. University of Warwick, on 21 May 2018 at 01:52:47, subject to the Cambridge Core terms of use, available at https://www.cambridge.org/core/terms. https://doi.org/10.1557/adv.2018.418

polymer compounds were used on the activation of CO_2 to reduce the thermodynamic energy barrier of electron transfer process of CO_2 reduction. The first process for activation of CO_2 is that forming the N-CO_2 bond by interaction between non-paired electron of N atoms and linear molecular structure of CO_2. The bent CO_2 get a dipole moment due to difference electron density in the structure caused by bent structure, reducing thermodynamical energy requirement for first electron transfer to result in $CO_2^{\cdot-}$. [32, 33]

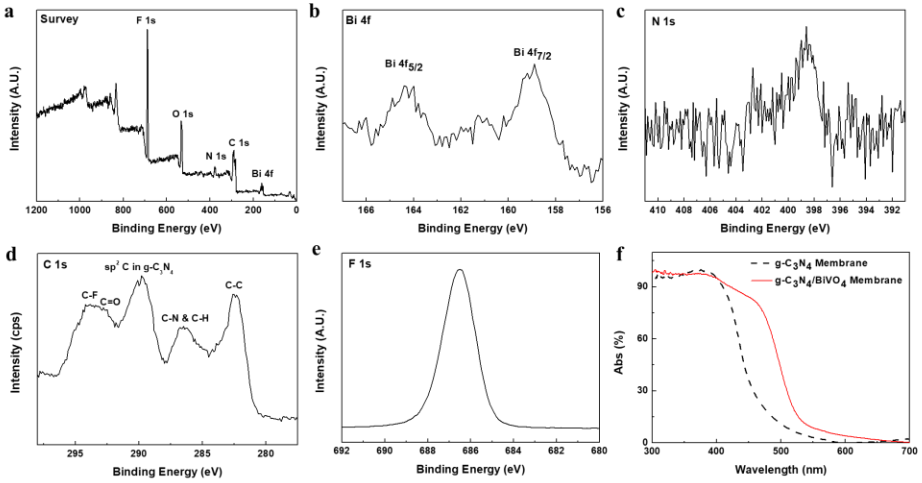

Figure 4. XPS spectra of g-C_3N_4/$BiVO_4$ multi-layered membrane catalyst (a) Survey, (b) Bi 4f, (c) N 1s, (d) C 1s and (e) F 1s. (f) UV-Vis spectra for g-C_3N_4 membrane catalyst and g-C_3N_4/$BiVO_4$ multi-layered membrane catalyst.

With the XPS analysis, Bi atom in the g-C_3N_4/$BiVO_4$ multi-layered membrane showed the binding energies at 164.7 eV for Bi $4f_{5/2}$ and 159 eV for Bi $4f_{7/2}$ (Figure 4b), which was well matched with the previous report on the binding state of Bi in $BiVO_4$.[34] In case of N atoms in the g-C_3N_4/$BiVO_4$ multi-layered membrane, the binding energy of N 1s showed at 398.2 eV for C-N=C bond and 399.4 eV for N-$(C)_3$ bond (Figure 4c), which was also well matched with the previous report on the binding state of N in g-C_3N_4.[35] In the C 1s spectra, C-C bond was measured at 283 eV, C-N bond from g-C_3N_4, sp^2 carbon from g-C_3N_4 and C-F bond from Nafion were showed at 287 eV and 289.5 eV, respectively (Figure 4d). The F 1s spectrum was also shown in Figure 4e with the C-F binding energy of 687 eV. The C 1s spectrum and F 1s spectrum were also well matched with previous reported XPS spectra of g-C_3N_4, $BiVO_4$ and Nafion.[36, 37] Those results were confirmed that major reaction sites of $BiVO_4$ and g-C_3N_4 were still remained as active binding state even after casting and shaping process of g-C_3N_4/$BiVO_4$ multi-layered membrane. Solar light absorption ability of g-C_3N_4 membrane catalyst was enhanced after fabrication of g-C_3N_4/$BiVO_4$ multi-layered membrane (Figure 4f). It was caused by the wider wave-length range solar light absorption ability of g-C_3N_4/$BiVO_4$ multi-layered membrane due to $BiVO_4$, compared with g-C_3N_4 only. The g-C_3N_4/$BiVO_4$ multi-layered membrane also resulted in an enhanced electron-hole charge separation by the interface junction between g C_3N_4 layer and $BiVO_4$ layer.

Downloaded from https://www.cambridge.org/core. University of Warwick, on 21 May 2018 at 01:52:47, subject to the Cambridge Core terms of use, available at https://www.cambridge.org/core/terms. https://doi.org/10.1557/adv.2018.418

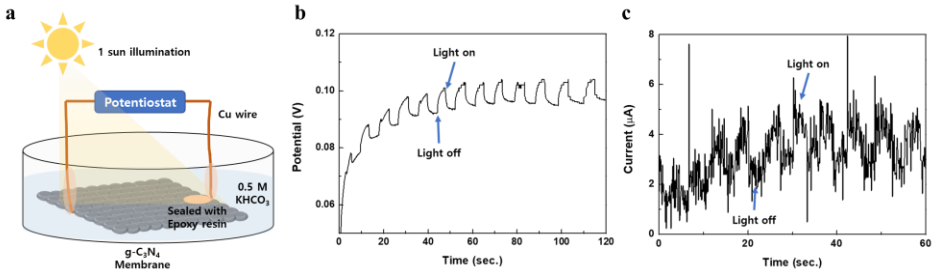

Figure 5. (a) Schematic drawing on the electrochemical measurement system, (b) transient V-t curve of g-C_3N_4 membrane and (c) transient j-t curve of g-C_3N_4 membrane.

To confirm that both g-C_3N_4 and $BiVO_4$ particles in the membrane catalyst are interfaced well enough to transport electrons from one layer to the other layer of the membrane catalysts, simple electrochemical analysis was performed. To prevent the short-circuit current, both contact points of Cu external wire with membrane in the electrolyte were sealed by epoxy resin. (Figure 5a) Within 2-electrode system, light induced potential of g-C_3N_4 membrane catalyst was measured with transient V-t curve. (Figure 5b) The potential generated in g-C_3N_4 membrane catalyst by one-sun irradiation was 50 mV. The appeared potential of g-C_3N_4 membrane catalyst on one-sun illumination was originated from electron-hole charge separation in g-C_3N_4 particle. Within a j-t curve, ~ 2 μA of current was generated from one-sun illumination. (Figure 5c) Considering photo-induced potential from electron-hole charge separation in g-C_3N_4 was 50 mV, low current value (~ 2 μA) was caused by resistivity in g-C_3N_4 membrane catalyst. The origin of the resistivity came from the intrinsic properties of Nafion polymer and generated charges were trapped at the interface junction area of g-C_3N_4 particles.

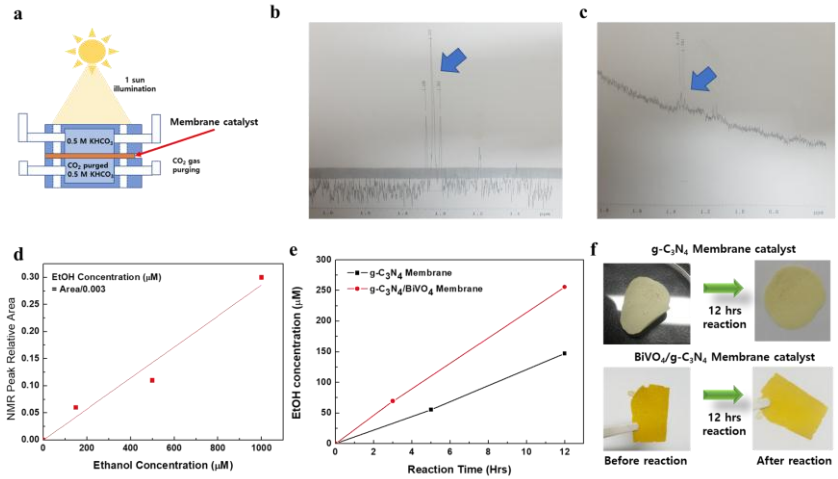

Figure 6. (a) Schematic drawing on the photochemical artificial photosynthesis cell using membrane catalysts, (b) NMR spectra of g-C_3N_4 membrane catalyst system after 5 hrs reaction, (c) NMR spectra of g-C_3N_4/$BiVO_4$ multi-layered membrane catalyst system after 12 hrs reaction, (d) Standard concentration calibration curves of ethanol by NMR, (e) Produced ethanol concentration versus time scale with g-C_3N_4 membrane catalyst and g-C_3N_4/$BiVO_4$ multi-layered membrane catalyst and (f) images of g-C_3N_4 membrane catalyst and g-C_3N_4/$BiVO_4$ multi-layered membrane catalyst before and after 12 hrs reaction.

Downloaded from https://www.cambridge.org/core. University of Warwick, on 21 May 2018 at 01:52:47, subject to the Cambridge Core terms of use, available at https://www.cambridge.org/core/terms. https://doi.org/10.1557/adv.2018.418

However, above photoelectrochemical analysis indicates that electron and proton pathways were well constructed, so the photogenerated charge can move through internal interface junction of the particles, finally it can reach on the surface of the other side of membrane catalyst, which is able to participate in the CO_2 reduction reaction.

The schematic drawing on the photochemical artificial photosynthesis cell using membrane catalysts are shown in Figure 6a. During the artificial photosynthesis reaction, CO_2 was purged only for CO_2 reduction reaction side of membrane catalyst. Both g-C_3N_4 membrane catalyst system and g-C_3N_4/$BiVO_4$ multi-layered membrane catalyst system, ethanol was detected as the major product in NMR analysis (Figure 6 b and c). The quantification of produced ethanol in both g-C_3N_4 membrane catalyst system and g-C_3N_4/$BiVO_4$ multi-layered membrane catalyst system was done by calculating ethanol concentration in product solution through relative NMR peak area-standard concentration of ethanol graph. In standard concentration calibration curves of ethanol are shown in Figure 6 d. The actual concentration of produced ethanol was quantified by dividing relative NMR peak area with 0.003, as following the standard concentration calibration curves. The concentration of ethanol in g-C_3N_4 membrane catalyst system was determined as 147 μM while a 256 μM of ethanol was determined in g-C_3N_4/$BiVO_4$ multi-layered membrane catalyst system after 12 hrs solar light irradiation. (Figure 6e) The fabricated g-C_3N_4 membrane catalyst and g-C_3N_4/$BiVO_4$ multi-layered membrane catalyst were stable enough to keep its own shape and flexibility after the artificial photosynthesis reaction for 12 hrs (Figure 6f).

CONCLUSIONS

In this work, we have tried the fabrication of polymer assisted photocatalytic membrane in the first time and advanced it to multi-layered membrane catalysts by facile method by stacking and pressing the different kinds of polymer layers for the catalytic membranes. The g-C_3N_4 synthesized by self-condensing method was used due to proper band position for water splitting and CO_2 reduction with CO_2 activation ability. $BiVO_4$ was used to enhance the water splitting efficiency through increasing light absorption and electron-hole charge separation ability. By fabricating g-C_3N_4/$BiVO_4$ multi-layered membrane catalyst, the produced concentration of ethanol by CO_2 reduction for 12 hrs through photochemical process was increased from 147 μM to 256 μM, with stability of membrane catalyst. This work suggests the new approach on fabricating efficient functional membrane system of artificial photosynthesis for CO_2 reduction into ethanol. In this system, solar water splitting reaction and CO_2 reduction reaction are separated from each other by Nafion membrane, preventing the re-oxidation of CO_2 reduction product in a simple way.

ACKNOWLEDGMENTS

This work was financially supported by the Korea Center for Artificial Photosynthesis (KCAP) located at Sogang University (No. 2009-0093885), which is funded by the Minister of Science, ICT and Future Planning (MSIP) through the National Research Foundation of Korea and the Brain Korea 21 Plus Project 2018.

Downloaded from https://www.cambridge.org/core. University of Warwick, on 21 May 2018 at 01:52:47, subject to the Cambridge Core terms of use, available at https://www.cambridge.org/core/terms. https://doi.org/10.1557/adv.2018.418

REFERENCES

1. A. Fujishima and K. Honda, *Nature* **238**, 37-38 (1972).
2. M. Graetzel, *Acc. Chem. Res.* **14**, 376-384 (1981).
3. A. Kudo and Y. Miseki, *Chem. Soc. Rev.* **38**, 253-278 (2009).
4. Y. Tachibana, L. Vayssieres and J.R. Durrant, *Nature Photonics* **6**, 511-518 (2012).
5. S.U.M. Khan, M. Al-Shahry and W.B. Ingler, *Science* **297**, 2243-2245 (2002).
6. C.W. Kim, S.J. Yeob, H.-M. Cheng and Y.S. Kang, *Energy Environ. Sci.* **8**, 3646-3653 (2015).
7. J.H. Park, S. Kim and A.J. Bard, *Nano Lett.* **6**, 24-28 (2006).
8. H.M. Chen, C.K. Chen, Y.C. Chang, C.W. Tsai, R.S. Liu, S.F. Hu, W.S. Chang and K.H. Chen, *Angew. Chem.* **122**, 6102-6105 (2010).
9. A.U. Pawar, C.W. Kim, M.J. Kang and Y.S. Kang, *Nano Energy* **20**, 156-167 (2016).
10. X. Yang, A. Wolcott, G. Wang, A. Sobo, R.C. Fitzmorris, F. Qian, J.Z. Zhang and Y. Li, *Nano Lett.* **9**, 2331-2336 (2009).
11. C.W. Kim, Y.S. Son, M.J. Kang, D.Y. Kim and Y.S. Kang, *Adv. Ener. Mater.* **6**, 1501754 (2016).
12. T.W. Kim and K.-S. Choi, *Science* **343**, 990-994 (2014).
13. B.M. Kayes, H. Nie, R. Twist, S.G. Spruytte, F. Reinhardt, I.C. Kizilyalli and G.S. Higashi: 27.6% Conversion efficiency, a new record for single-junction solar cells under 1 sun illumination, in 2011 37th IEEE Photovoltaic Specialists Conference (2011), pp. 4-8.
14. O. Khaselev and J.A. Turner, *Science* **280**, 425-427 (1998).
15. K. Sivula, F.L. Formal and M. Grätzel, *Chem. Mater.* **21**, 2862-2867 (2009).
16. J. Su, L. Guo, N. Bao and C.A. Grimes, *Nano Lett.* **11**, 1928-1933 (2011).
17. J.Y. Zheng, Z. Haider, T.K. Van, A.U. Pawar, M.J. Kang, C.W. Kim and Y.S. Kang, *CrystEngComm* **17**, 6070-6093 (2015).
18. M. Sathish, B. Viswanathan and R.P. Viswanath, *Int. J. Hydrogen Energy* **31**, 891-898 (2006).
19. Y. Xu, W. Zhao, R. Xu, Y. Shi and B. Zhang, *Chem. Commun.* **49**, 9803-9805 (2013).
20. J.H. Kim, J.-W. Jang, Y.H. Jo, F.F. Abdi, Y.H. Lee, R. van de Krol and J.S. Lee, *Nature Comm.* **7**, 13380 (2016).
21. M.R. Singh, E.L. Clark and A.T. Bell, *PNAS* **112**, E6111-E6118 (2015).
22. C.W. Kim, M.J. Kang, S. Ji and Y.S. Kang, *ACS Catal.* **8**, 968-974 (2018).
23. Q. Kong, D. Kim, C. Liu, Y. Yu, Y. Su, Y. Li and P. Yang, *Nano Lett.* **16**, 5675-5680 (2016).
24. S. Wang and X. Wang, *Appl. Catal., B: Environ.* **162**, 494-500 (2015).
25. Y.-F. Xu, M.-Z. Yang, B.-X. Chen, X.-D. Wang, H.-Y. Chen, D.-B. Kuang and C.-Y. Su, *J. Am. Chem. Soc.* **139**, 5660-5663 (2017).
26. H. Li, Y. Gao, Y. Zhou, F. Fan, Q. Han, Q. Xu, X. Wang, M. Xiao, C. Li and Z. Zou, *Nano Lett.* **16**, 5547-5552 (2016).
27. H. Li, W. Tu, Y. Zhou and Z. Zou, *Adv. Sci.* **3**, 1500389 (2016).
28. S. Ye, R. Wang, M.-Z. Wu and Y.-P. Yuan, *Appl. Surf. Sci.* **358**, 15-27 (2015).
29. S.J. Paddison and R. Paul, *PCCP* **4**, 1158-1163 (2002).
30. J. Maiti, N. Kakati, S.P. Woo and Y.S. Yoon, *Compos. Sci. Technol.* **155**, 189-196 (2018).
31. L. Huang, Y. Li, H. Xu, Y. Xu, J. Xia, K. Wang, H. Li and X. Cheng, *RSC Adv.* **3**, 22269-22279 (2013).
32. E.E. Barton, D.M. Rampulla and A.B. Bocarsly, *J. Am. Chem. Soc.* **130**, 6342-6344 (2008).
33. H. Jeong, M.J. Kang, H. Jung and Y.S. Kang, *Faraday Discuss.* **198**, 409-418 (2017).
34. J. Gan, X. Lu, B.B. Rajeeva, R. Menz, Y. Tong and Y. Zheng, *ChemElectroChem* **2**, 1385-1395 (2015).
35. L. Shen, Z. Xing, J. Zou, Z. Li, X. Wu, Y. Zhang, Q. Zhu, S. Yang and W. Zhou, *Scientific Reports* **7**, 41978 (2017).
36. T.Y. Ma, S. Dai, M. Jaroniec and S.Z. Qiao, *Angew. Chem.* **126**, 7409-7413 (2014).
37. H. Yang, S. Zhang, R. Cao, X. Deng, Z. Li and X. Xu, *Sci. Rep.* **7**, 8686 (2017).

Downloaded from https://www.cambridge.org/core. University of Warwick, on 21 May 2018 at 01:52:47, subject to the Cambridge Core terms of use, available at https://www.cambridge.org/core/terms. https://doi.org/10.1557/adv.2018.418